Searching quantum entanglement in the $pp \to ZZ$ process*

Alim Ruzi (阿里木·肉孜)† Youpeng Wu (吴友鹏)‡ Ran Ding (丁然)§ Qiang Li (李强)♮

State Key Laboratory of Nuclear Physics and Technology, School of Physics, Peking University, Beijing 100871, China

Abstract: Recent studies have shown that observing entangled particle states at a particle collider, such as the Large Hadron Collider (LHC), and testing the violation of Bell inequality in them can open up new research areas for studying high energy physics. We examine the presence of quantum entanglement in the $pp \to ZZ \to 4\ell$ process at leading order. We apply a generally recognized method, quantum state tomography, to reconstruct the spin density matrix of the joint ZZ system, through which all the relevant observables can be obtained. The angular distribution of the final leptons is obtained from simulated events using a Monte-Carlo program, which is used to reconstruct the spin density matrix. A non-zero value of the lower bound of the concurrence is measured with the simulated data. The numerical analysis shows that, with the luminosity corresponding to LHC Run 2+3, entanglement can be probed at the 2 σ level and up to the 3.75σ level for High-Luminosity LHC data (3ab^{-1}), revealing the possibility of finding quantum entanglement in real collider experiments.

Keywords: quantum entanglement, high energy physics, electroweak di-boson production, TeV collider

DOI: 10.1088/1674-1137/ae1374 **CSTR:** 32044.14.ChinesePhysicsC.50023103

I. INTRODUCTION

Quantum entanglement [1], a cornerstone of quantum mechanics, represents a fascinating phenomenon where two or more particles become intricately correlated, such that the change in one particle's quantum state instantaneously influences the state of the other, termed as "spooky action at a distance" by Einstein *et al.* [2]. This phenomenon might be the most outstanding characteristic of quantum mechanics that truly separates quantum mechanics from classical deterministic theory. This could be proven by testing the violation of Bell inequalities [3] using the theory of quantum mechanics, which is unfeasible within any theory that advocates local realism.

Studies on the quantum entanglement of multi-particle systems at the highest energy frontiers of particle physics have recently gained considerable interest among both theorists and experimentalists. There have been breakthroughs in the study of quantum entanglement and quantum information science at the high energy frontier [4−11]. For example, several studies show that a violation of Bell inequality could be measured in heavy quark systems, *i.e.*, $t\bar{t}$, $b\bar{b}$ at the Large Hadron Collider (LHC) [12−25]. Considering the heavy mass and very short life time, the $t\bar{t}$ system can be an ideal platform to perform quantum tests at the LHC. Both the ATLAS and CMS collaborations [26−28] have measured entanglement among top quark pairs with a high sensitivity. So far, searches for quantum entanglement and the testing of Bell nonlocality between other pairs of systems have continuously gained attention at collider experiments.

Quantum state tomography [29−31], determining the density matrix from an ensemble of measurements, has emerged as a cornerstone technique for reconstructing the quantum state of a system, providing invaluable insights into quantum correlations, coherence, and entanglement [32−35]. While initially developed within the realm of quantum optics and low-dimensional systems, advancements in experimental and theoretical physics have extended its applicability to high-energy particle physics, particularly in exploring the quantum properties of massive gauge particles produced at particle colliders [36−52]. The advent of high-energy colliders, such as the LHC and the proposed muon collider, opens a promising avenue

Received 12 August 2025; Accepted 10 October 2025; Accepted manuscript online 11 October 2025

* Supported by National Natural Science Foundation of China (NSFC) (12325504, 120611410), and by MOST (2023YFA1605800). This work is supported in part by the National Natural Science Foundation of China (12325504, 12150005, 12075004)

† E-mail: alim.ruzi@pku.edu.cn
‡ E-mail: youpeng@stu.pku.edu.cn (Corresponding author)
§ E-mail: ran.ding@cern.ch
♮ E-mail: qliphy0@pku.edu.cn

for probing the fundamental aspects of quantum mechanics in previously inaccessible regimes.

The study of massive spin-1 particles, such as the electroweak gauge bosons *WW* and *ZZ*, is particularly compelling in this context. These particles play a critical role in the standard model of particle physics, mediating weak interactions and participating in processes that probe electroweak symmetry breaking [53−56]. At a muon collider [57, 58], where precise beam properties and high luminosity enable clean experimental conditions, the production of such particles offers an unparalleled opportunity to investigate their quantum properties. Specifically, the quantum state tomography of *WW* and *ZZ* boson pairs provides a direct method to study their spin correlations, polarization states, and entanglement, enriching our understanding of the quantum nature of the standard model.

In this study, we explore the quantum properties of the *ZZ* system, such as quantum correlation and concurrence, and check the separability of this state. This is realized through the quantum state tomography of two massive spin-1 particles produced in a 13 TeV proton-proton collision, whose spin density matrix is determined from the simulated events of $pp\to ZZ\to 4\ell$. Quantum observables, such as concurrence, are measured to examine whether the *ZZ* pairs are entangled or separable in such an extremely relativistic environment.

II. QUANTUM STATE TOMOGRAPHY AND QUANTUM ENTANGLEMENT

A. Spin density matrix for *ZZ* system

A spin density matrix is a mathematical structure that describes the quantum state of a given system, including both pure and mixed states and encapsulating all the observables related to quantum information, such as concurrence [59], quantum discord [60], quantum magic [61], and entanglement entropy [62]. In quantum mechanics, the state vector $|\Psi\rangle$ is dominantly used to describe the quantum mechanical state of the corresponding system. For a pure state, the spin density matrix, $\rho=|\Psi\rangle\langle\Psi|$, has the equivalent role as $|\Psi\rangle$, whereas for a mixed state, the spin density matrix is defined as the convex sum

$$\rho=\sum_i p_i|\psi_i\rangle\langle\psi_i|, \tag{1}$$

where p_i is the classical probability of the i-th pure state $|\psi_i\rangle$ and satisfies $\sum p_i=1$. The density matrix is a positive semi-definite operator, which indicates $\langle i|\rho|i\rangle$, where $|i\rangle$ is the base state in the complex Hilbert space $\mathcal{H}$. The total sum probabilities p_i in Eq. (1) result from the requirement that ρ must have unit trace.

To reconstruct the spin density matrix from experimental or simulated pseudo data, it must be parametrized. As known in the spin context of quantum mechanics, the Pauli spin matrix σ_i is usually chosen to parametrize the spin density matrix of an $s=1/2$ system, which constitutes a qubit. For example, the following form of spin density matrix for a two-qubit system is parametrized with σ_i:

$$\rho=\frac{1}{4}\left[I_2\otimes I_2+\sum_{i=1}^{3}(A_i\sigma_i\otimes I_2+B_iI_2\otimes\sigma_i)+\sum_{i,j=1}^{3}C_{ij}\sigma_i\otimes\sigma_j\right], \tag{2}$$

where A_i and B_i are the components of the polarization vector of each qubit, and C_{ij} is the entry of the correlation matrix. For any two-qutrit system composed of two spin-1 particles, the general spin density matrix can be represented using traceless Gell-Mann matrices as follows [63]:

$$\begin{aligned}\rho=&\frac{1}{9}[I_3\otimes I_3]+\sum_{i=1}^{8}A_i[T^i\otimes I_3]\\&+\sum_{i=1}^{8}B_i[I_3\otimes T^i]+\sum_{i,j=1}^{8}C_{ij}[T^i\otimes T^j],\end{aligned} \tag{3}$$

where T^i are 3×3 Gell-Mann matrices with $i=1,2,\ldots,8$, and I_3 is a three-dimensional identity matrix. The coefficients A_i, B_i are spin polarization parameters or the components of the polarization for each qutrit, and C_{ij} represents the spin correlation parameters. These parameters can be obtained by projecting the spin density matrix on the desired subspace basis as

$$\begin{aligned}&A_i=\frac{1}{6}\mathrm{Tr}\left[\rho T_i\otimes I_3\right],\quad B_i=\frac{1}{6}\mathrm{Tr}\left[\rho I_3\otimes T_i\right],\\&C_{ij}=\frac{1}{4}\mathrm{Tr}\left[\rho T_i\otimes T_j\right].\end{aligned} \tag{4}$$

Analytically, the obtained coefficients in Eq. (4) are Lorentz invariant and depend only on the energy E, momentum, or velocity, and the scattering angle in the CM frame. Once these coefficients are known, it is straightforward to determine the observables quantifying the entanglement in the massive gauge boson system.

B. Entanglement observables

Quantifying the entanglement of the state of a quantum system is generally challenging as the complexity of the problem increases with the system dimensionality. For a pure state described by a single vector in the Hilbert space, or equivalently by a density matrix, this can be solved by its Schmidt decomposition [1]. As for mixed states, a general approach is to compute the so-called entanglement witness, a quantity that provides sufficient conditions to establish the presence of entanglement in the system. Such an observable quantity is concurrence, which has been mentioned in the above section. This is a reliable entanglement measure for a bipartite system consisting of two particles [64, 65].

Usually, for a pure state described by a joint-state vector, the corresponding concurrence is defined as

$$C[|\psi\rangle] = \sqrt{2(1-\mathrm{Tr}[(\rho_r)^2])}, \tag{5}$$

where ρ_r is the reduced density matrix of the subsystem obtained by tracing over the degree of freedom of either subsystem. However, the concurrence of any mixed state described by Eq. (1) is given by the concurrence of the pure states as

$$C(\rho) = \inf_{\{|\psi_i\rangle\}} \sum_i p_i C(|\psi_i\rangle), \tag{6}$$

where an infimum is taken over all the possible decompositions of ρ into pure states. A vanishing value of Eq. (5) indicates that the pure state of the bipartite system is separable. However, owing to the complexity in the evolution of mixed states, evaluating its concurrence, Eq. (6), to a specific value is challenging. Therefore, finding a lower bound of concurrence for mixed states, rather than obtaining the exact value, also unequivocally indicates the presence of entanglement. This lower bound is analytically computable [66, 67]:

$$[C(\rho)]^2 \geq \mathscr{C}_2[\rho] = 2\max(0, \mathrm{Tr}[\rho^2] - \mathrm{Tr}[(\rho_A)^2], \mathrm{Tr}[\rho^2] - \mathrm{Tr}[(\rho_B)^2]), \tag{7}$$

or equivalently, the above lower bound can be written for a two-qutrit system of spin-1 massive bosons as

$$\mathscr{C}_2[\rho] = 2\mathrm{Tr}[\rho]^2 - \mathrm{Tr}[\rho_A^2] - \mathrm{Tr}[\rho_B^2] \equiv c_{\mathrm{MB}}^2. \tag{8}$$

By using the explicit form of the spin density matrix parametrized as Eq. (2), the lower bound of concurrence $\mathscr{C}_2$ can be written in terms of the coefficients given in Eq. (4):

$$c_{\mathrm{MB}}^2 = -\frac{4}{9} - 6\sum_i A_i^2 - 6\sum_i B_i^2 + 8\sum_{ij} C_{ij}^2. \tag{9}$$

The state is entangled if the above quantity is positive, whereas if the lower bound is negative or equal to zero, the concurrence test is inconclusive.

C. Extraction of spin density matrix from data

Owing to its short lifetime, the Z boson cannot be detected directly inside the detector. The most abundant decay channel is hadronic decay, which accounts for up to 70% of the total decay. The leptonic decay channel is convenient to manipulate both in the simulation and actual experiments. The information about the entanglement of the states is passed to the decay products, namely, charged leptons. The angular direction of each of these leptons is correlated with the direction of the spin of their parent Z boson in such a way that the normalized differential cross-section of the process $ZZ \to \ell_1^+\ell_1^-\ell_2^+\ell_2^-$ may be written as [68]

$$\frac{1}{\sigma}\frac{\mathrm{d}\sigma}{\mathrm{d}\Omega^+\mathrm{d}\Omega^-} = \left(\frac{3}{4\pi}\right)^2 \mathrm{Tr}\left[\rho_{V_1V_2}(\Gamma_1 \otimes \Gamma_2)\right] \tag{10}$$

in which the solid angle measure $\mathrm{d}\Omega^{\pm} = \sin\theta^{\pm}\mathrm{d}\theta^{\pm}\mathrm{d}\phi^{\pm}$ is written in terms of the spherical coordinates for the momenta of the final charged leptons in the respective rest frame of the decaying particles. The density matrix $\rho_{V_1V_2}$ encodes the production information of the joint ZZ system, whereas the decay density matrix Γ_i passes the relevant entanglement information about the ZZ state to the final decay products, so that we can recover the spin density matrix from this angular distribution. The explicit form of the decay density matrix Γ_i can be obtained using polarized decay amplitudes [68]

$$\Gamma = \frac{1}{4}\begin{pmatrix} 1+\cos^2\theta - 2\eta_\ell\cos\theta & \frac{1}{\sqrt{2}}(\sin 2\theta - 2\eta_\ell\sin\theta)\mathrm{e}^{\mathrm{i}\varphi} & (1-\cos^2\theta)\mathrm{e}^{\mathrm{i}2\varphi} \\ \frac{1}{\sqrt{2}}(\sin 2\theta - 2\eta_\ell\sin\theta)\mathrm{e}^{-\mathrm{i}\varphi} & 2\sin^2\theta & -\frac{1}{\sqrt{2}}(\sin 2\theta + 2\eta_\ell\sin\theta)\mathrm{e}^{\mathrm{i}\varphi} \\ (1-\cos^2\theta)\mathrm{e}^{-\mathrm{i}2\varphi} & -\frac{1}{\sqrt{2}}(\sin 2\theta + 2\eta_\ell\sin\theta)\mathrm{e}^{-\mathrm{i}\varphi} & 1+\cos^2\theta - 2\eta_\ell\cos\theta \end{pmatrix}, \tag{11}$$

where θ and ϕ are the polar angles of the momentum of the negative charged lepton in the rest frame of the mother particle, which is a Z boson. η_ℓ is a function of the electroweak mixing angle [69] and is equal to 0.15 when using the latest measurement of the mixing angle [70].

The functions given in Eq. (A2), together with the matrix A_i^j (A3) in Appendix, can be used to extract the polarization and correlation coefficients of the density matrix given in Eq. (3):

$$\hat{A}_i = \frac{1}{6}\left\langle \tilde{p}_i^1(\hat{\mathbf{n}}_1)\right\rangle, \quad \hat{B}_i = \frac{1}{6}\left\langle \tilde{p}_i^2(\hat{\mathbf{n}}_2)\right\rangle,$$
$$\hat{C}_{ij} = \frac{1}{4}\left\langle \tilde{p}_i^1(\hat{\mathbf{n}}_1) p_j^2(\hat{\mathbf{n}}_2)\right\rangle, \tag{12}$$

where $\tilde{p}$ is the corresponding Wigner P symbol for Z boson decay, and is given as

$$\tilde{p}_i = \sum_{j=1}^{8} A_i^j p_j^+. \tag{13}$$

The unit vector $\hat{\mathbf{n}}(\theta,\phi)$ in Eq. (12) is defined for the momentum of the decay leptons in the rest frame. As the two Z bosons are indistinguishable, a symmetry factor should be implied by exchanging the labels i and j, so that the above coefficients are determined as

$$\hat{A}_i = \hat{B}_i = \frac{1}{12}\left\langle p_i^1(\hat{\mathbf{n}}_1) + p_i^2(\hat{\mathbf{n}}_2)\right\rangle,$$
$$\hat{C}_{ij} = \frac{1}{8}\left\langle p_i^1(\hat{\mathbf{n}}_1) p_j^2(\hat{\mathbf{n}}_2) + p_j^1(\hat{\mathbf{n}}_1) p_i^2(\hat{\mathbf{n}}_2)\right\rangle. \tag{14}$$

Eq. (14) allows us to reconstruct the correlation functions for the density matrix from the distribution of the lepton momenta and thus allows us to derive the expectation value of the lower bound of concurrence $\mathscr{C}_2$ from the data.

III. SIMULATION AND NUMERICAL RESULTS

A sensitivity test for the entanglement content is performed through pseudo-experiments of the $pp \to ZZ$ process at the LHC with a center-of-mass energy of $\sqrt{s} = 13$ TeV. Unlike massive gauge boson pair production in the Higgs decay, in which one of the gauge bosons is produced off-shell, here, both ZZ bosons are produced on-shell. The Feynman diagram of the $pp \to ZZ$ process, in which $Z \to \ell^+\ell^-$ $(\ell = e,\mu)$, where ℓ can be either an electron or a muon, is shown in Fig. 1. This is the signal process in our study. Simulation is conducted through publicly available Monte-Carlo software `MadGraph5_aMC@NLO` [71]. The relevant spin-correlation and Breit-Wigner effects are included through the `MadSpin` program [72, 73], which includes `MadGraph5_aMC@NLO`.

The number of generated events and corresponding cross sections are given in Table 1. The relevant cross sections are computed using `MadGraph5_aMC@NLO` at the leading order (LO) level. The center-of-mass energy (CM) is set to $\sqrt{s} = 13$ TeV for three different collider luminosities corresponding to the LHC Run 2+3 and HL-LHC luminosities. When calculating the cross section for both the signal and background processes, we use the default parton distribution function (PDF) set `NNPDF23` [74] and set the factorization and normalization scale to the physical mass of the Z boson.

As for the possible background processes, we consider the following three processes as background to our signal:

- $pp \to WWZ$
- $pp \to WZZ$
- $pp \to ZZZ$

Figure 2 depicts the event distributions for both the signal and total backgrounds as functions of the invariant mass of the final four leptons. The background events do not matter in the signal region. Thus, we can safely ignore any contamination from the background events. The $pp \to ZZ$ signal process exhibits strong background suppression owing to the reconstruction of the ZZ pair via isolated leptons, resulting in minimal background contamination. The dominant background, WWZ, involves two W bosons decaying to a charged lepton and the corresponding neutrino, leading to a broad four-lepton invariant mass ($M_{4\ell}$) distribution. This distinct kinematic feature allows clear separation from the narrow resonance of the ZZ signal. The final leptons originating from the Z boson pairs can be identified as two electrons and two muons, four electrons, or four muons. For two elec-

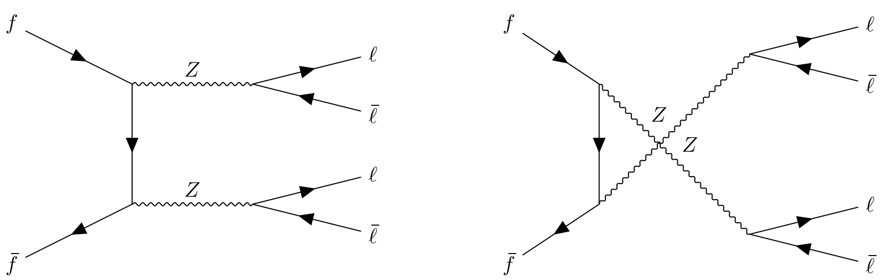

Fig. 1. Feynman diagram of the $pp \to ZZ$ process.

Table 1. Signal and background processes considered in this study in the first column, total cross section in the second column, and event numbers given for the total luminosity.

Process	Cross section (fb)	Events(Lumi=137 fb^{-1})	Events(Lumi=300 fb^{-1})	Events(Lumi=3 ab^{-1})
$p\,p \to ZZ$(signal)	42.29	5793	12687	126870
ZZZ	24.16	3309	7248	72480
WWZ	29.76	4077	8928	89280

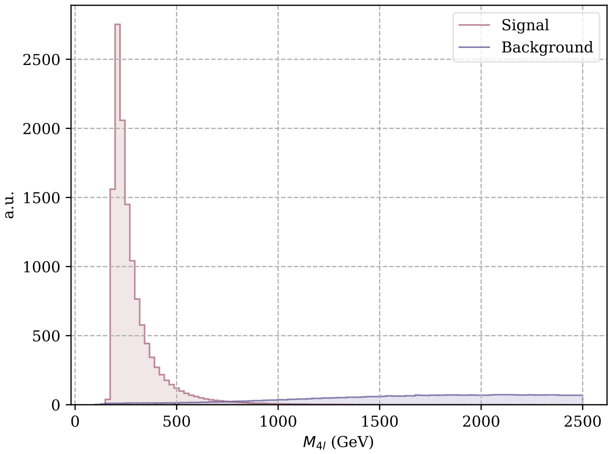

Fig. 2. (color online) Event distribution of the signal and background processes.

trons and two muons, it is easy to distinguish their parent Z boson. In the case where the ZZ system decays into four same-flavor leptons, we distinguish the signal by combinations: we iterate through all possible lepton pairings and select the combination in which the invariant mass of the reconstructed Z boson is closest to the on-shell mass. This strategy is effective because both Z bosons in the signal process are on-shell. In the numerical calculation, we extract the polarization and correlation coefficients of the spin density matrix from each single event using Wigner P symbols. Implementing this procedure over all the events provides the average value and standard deviation of our observables. We produce one million events in total and divide them into 1000 pseudo experiments, each one including events that match the total reachable events in actual experiments. The statistical uncertainty is determined with these pseudo experiments by repeating across all the pseudo experiments. The parameters of the spin density matrix, A_i, B_i, and C_{ij}, are shown in a matrix plot depicted in Fig. 3. There are several non-zero coefficients, indicating the correlations between the two Z bosons. The concurrence observable that quantifies entanglement is given as the function of $\cos\theta$, which is depicted in Fig. 4. For the Run 2+3 data, indicated by the gray band, the computed lower bound of the concurrence is relatively larger than one, which is unphysical, whereas it is close to unity when $\theta \to 0$ or π. However, the HL-LHC data, indicated by the colored band, provide physical results when the scattering aligns with the beam direction.

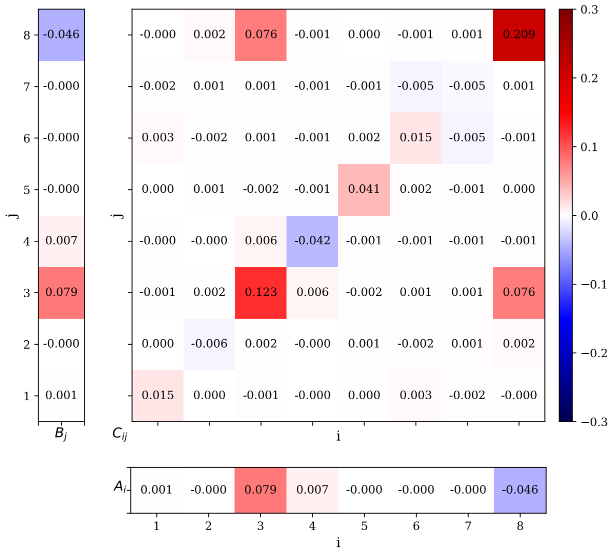

Fig. 3. (color online) Correlation matrix element extracted from the simulated data of ZZ production. The leftmost column shows the A_i parameters of the Z boson, the bottom row shows the parameters B_i, and the center middle table plot shows the C_{ij} coefficients.

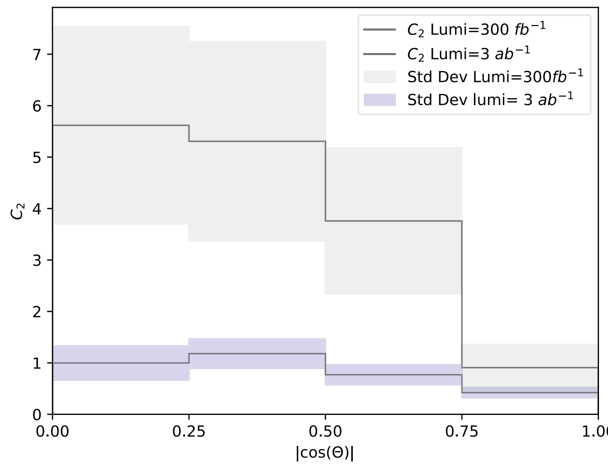

Fig. 4. (color online) Concurrence distribution as a function of the scattering angle cosine $\cos\theta$. The thick central lines are the central values, and the colored bands represent statistical deviations obtained from events corresponding to the LHC Run 2+3 and HL-LHC luminosities.

Because of the high event numbers, the uncertainty of the concurrence for this run is also small. The quantum entanglement test has a highly statistical meaning, which indicates that the results computed for the observables at hand, both the mean and deviation, are dependent on the event numbers in the actual experiments. To confirm this statistical nature of the entanglement, a Gaussian distribution of the lower bound of the concurrence, $C^2_{\rm MB}$, is obtained corresponding to the LHC Run 2+3 and HL-LHC luminosities. The results are shown in Fig. 5. The $C^2_{\rm MB}$ distribution converges to the mean value depicted by the red-dashed line for the HL-LHC data, whereas it diverges for the Run 2+3 data.

Based on the distributed results shown in Fig. 5, the expectation value of the $C^2_{\rm MB}$ observable converges to some point when the luminosity of the collider increases. To perform a test, we compute a luminosity spectrum for $C^2_{\rm MB}$, and the results are shown in the left panel of Fig. 6: the points indicate the expectation values, and the error bar indicates the uncertainty. $C^2_{\rm MB}$ converges approximately to 0.375 as the luminosity increases. Meanwhile, the corresponding significance can reach 3.75 σ for the HL-LHC luminosity, which is shown in the right panel of Fig. 6. This is well-above the 3σ confidence level.

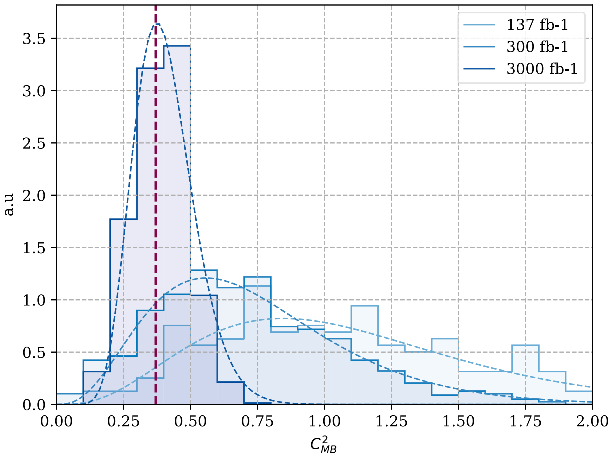

Fig. 5. (color online) $C^2_{\rm MB}$ distribution computed from the LHC Run 2+3 and HL-LHC luminosity data. The red dashed line is the mean value obtained from HL-LHC luminosity.

IV. SUMMARY

Quantum entanglement is one of the most distinctive features of quantum mechanics. It is being widely examined and tested by the particle physics community, especially the high energy physics frontiers, such as at the LHC and future colliders. In this study, we applied quantum state tomography to the *ZZ* system to examine the presence of quantum entanglement in the $pp \to ZZ \to 4\ell$ process. The theoretical framework by which the spin density matrix is computed or parametrized for the *ZZ* system is given, and a thorough explanation of the quantum state tomography is provided.

Importantly, a fast Monte-Carlo simulation of $pp \to ZZ$ is performed using `MadGraph5_aMC@NLO` software so that a large number of pseudo experiments can be used to determine whether quantum entanglement exists in the *ZZ* state. Accordingly, first, Gell-Mann spin matrices are used to parameterize the spin density matrix. Second, one million events corresponding to the LHC Run 2+3 and HL-LHC luminosities are produced for the $pp \to ZZ$ process for the LHC Run 2+3 and HL-LHC luminosity, based on which the total events are sliced into 1000 pseudo experiments. Then, using the theoretical framework, all the coefficients of the spin density matrix are determined by the angular distribution of the final lepton pairs originating from the *Z* boson decay. An entanglement quantifier, that is, the lower bound of the concurrence, is measured using these pseudo experiments. The significance of this quantity can reach 2σ with combined LHC Run 2+3 data and 3.75 σ for HL-LHC data, making it possible to measure quantum entanglement between two massive gauge boson pairs in an actual LHC experiment.

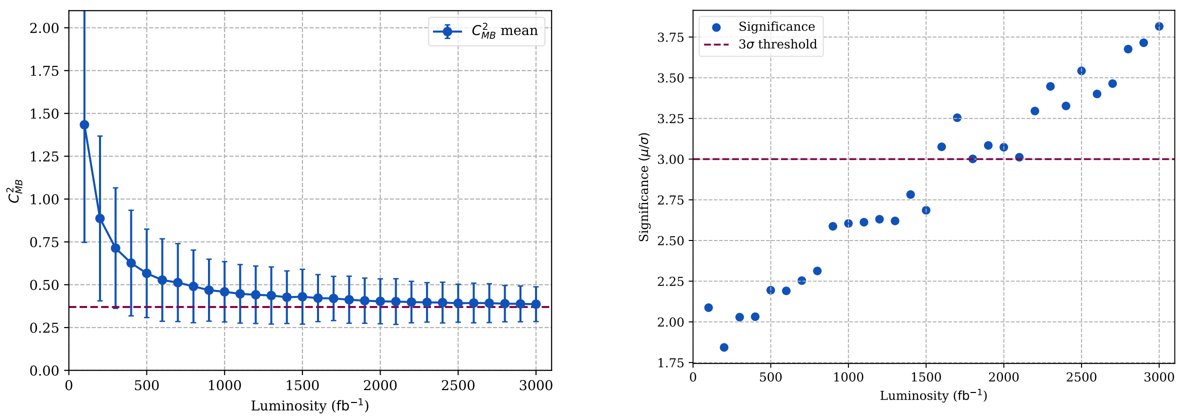

Fig. 6. (color online) Expectation value (left panel) of $C^2_{\rm MB}$ as a function of collider luminosity, and significance distribution (right panel)

APPENDIX A: THE FUNCTIONS $\mathfrak{q}_\pm^n$ AND $\mathfrak{p}_\pm^n$

The functions $\mathfrak{q}_\pm^n$ and $\mathfrak{p}$ are defined as follows according to [75, 76]:

$$
\begin{aligned}
\mathfrak{q}_\pm^1 &= \frac{1}{\sqrt{2}} \sin\theta^\pm \left(\cos\theta^\pm \pm 1\right) \cos\phi^\pm, \\
\mathfrak{q}_\pm^2 &= \frac{1}{\sqrt{2}} \sin\theta^\pm \left(\cos\theta^\pm \pm 1\right) \sin\phi^\pm, \\
\mathfrak{q}_\pm^3 &= \frac{1}{8} \left(1 \pm 4\cos\theta^\pm + 3\cos 2\theta^\pm\right), \\
\mathfrak{q}_\pm^4 &= \frac{1}{2} \sin^2\theta^\pm \cos 2\phi^\pm, \\
\mathfrak{q}_\pm^5 &= \frac{1}{2} \sin^2\theta^\pm \sin 2\phi^\pm, \\
\mathfrak{q}_\pm^6 &= \frac{1}{\sqrt{2}} \sin\theta^\pm \left(-\cos\theta^\pm \pm 1\right) \cos\phi^\pm, \\
\mathfrak{q}_\pm^7 &= \frac{1}{\sqrt{2}} \sin\theta^\pm \left(-\cos\theta^\pm \pm 1\right) \sin\phi^\pm, \\
\mathfrak{q}_\pm^8 &= \frac{1}{8\sqrt{3}} \left(-1 \pm 12\cos\theta^\pm - 3\cos 2\theta^\pm\right),
\end{aligned} \tag{A1}
$$

where $\theta^\pm$ and $\phi^\pm$ are the polar and azimuthal angles of the decay lepton $l^\pm$ in the Z boson rest frame, respectively. The function $\mathfrak{p}$ is defined as

$$
\begin{aligned}
\mathfrak{p}_\pm^1 &= \sqrt{2} \sin\theta^\pm \left(5\cos\theta^\pm \pm 1\right) \cos\phi^\pm, \\
\mathfrak{p}_\pm^2 &= \sqrt{2} \sin\theta^\pm \left(5\cos\theta^\pm \pm 1\right) \sin\phi^\pm, \\
\mathfrak{p}_\pm^3 &= \frac{1}{4} \left(5 \pm 4\cos\theta^\pm + 15\cos 2\theta^\pm\right), \\
\mathfrak{p}_\pm^4 &= 5\sin^2\theta^\pm \cos 2\phi^\pm, \\
\mathfrak{p}_\pm^5 &= 5\sin^2\theta^\pm \sin 2\phi^\pm, \\
\mathfrak{p}_\pm^6 &= \sqrt{2} \sin\theta^\pm \left(-5\cos\theta^\pm \pm 1\right) \cos\phi^\pm, \\
\mathfrak{p}_\pm^7 &= \sqrt{2} \sin\theta^\pm \left(-5\cos\theta^\pm \pm 1\right) \sin\phi^\pm, \\
\mathfrak{p}_\pm^8 &= \frac{1}{4\sqrt{3}} \left(-5 \pm 12\cos\theta^\pm - 15\cos 2\theta^\pm\right).
\end{aligned} \tag{A2}
$$

The matrix $\mathfrak{a}_m^n$ is defined as

$$
\mathfrak{a}_m^n = \frac{1}{g_L^2 - g_R^2}
\begin{bmatrix}
g_R^2 & 0 & 0 & 0 & 0 & g_L^2 & 0 & 0 \\
0 & g_R^2 & 0 & 0 & 0 & 0 & g_L^2 & 0 \\
0 & 0 & g_R^2 - \frac{1}{2} g_L^2 & 0 & 0 & 0 & 0 & \frac{\sqrt{3}}{2} g_L^2 \\
0 & 0 & 0 & g_R^2 - g_L^2 & 0 & 0 & 0 & 0 \\
0 & 0 & 0 & 0 & g_R^2 - g_L^2 & 0 & 0 & 0 \\
g_L^2 & 0 & 0 & 0 & 0 & g_R^2 & 0 & 0 \\
0 & g_L^2 & 0 & 0 & 0 & 0 & g_R^2 & 0 \\
0 & 0 & \frac{\sqrt{3}}{2} g_L^2 & 0 & 0 & 0 & 0 & g_L^2 - \frac{1}{2} g_R^2
\end{bmatrix} \tag{A3}
$$

APPENDIX B: GELL-MANN MATRICES

The 3×3 Gell-Mann matrices are defined as

$$
\mathbb{1} = \begin{bmatrix} 1 & 0 & 0 \\ 0 & 1 & 0 \\ 0 & 0 & 1 \end{bmatrix}, \quad
T^1 = \begin{bmatrix} 0 & 1 & 0 \\ 1 & 0 & 0 \\ 0 & 0 & 0 \end{bmatrix}, \quad
T^2 = \begin{bmatrix} 0 & -\mathrm{i} & 0 \\ \mathrm{i} & 0 & 0 \\ 0 & 0 & 0 \end{bmatrix},
$$

$$
T^3 = \begin{bmatrix} 1 & 0 & 0 \\ 0 & -1 & 0 \\ 0 & 0 & 0 \end{bmatrix}, \quad
T^4 = \begin{bmatrix} 0 & 0 & 1 \\ 0 & 0 & 0 \\ 1 & 0 & 0 \end{bmatrix}, \quad
T^5 = \begin{bmatrix} 0 & 0 & -\mathrm{i} \\ 0 & 0 & 0 \\ \mathrm{i} & 0 & 0 \end{bmatrix},
$$

$$
T^6 = \begin{bmatrix} 0 & 0 & 0 \\ 0 & 0 & 1 \\ 0 & 1 & 0 \end{bmatrix}, \quad
T^7 = \begin{bmatrix} 0 & 0 & 0 \\ 0 & 0 & -\mathrm{i} \\ 0 & \mathrm{i} & 0 \end{bmatrix}, \quad
T^8 = \frac{1}{\sqrt{3}} \begin{bmatrix} 1 & 0 & 0 \\ 0 & 1 & 0 \\ 0 & 0 & -2 \end{bmatrix}
$$

References

[1] R. Horodecki, P. Horodecki, M. Horodecki *et al.*, Rev. Mod. Phys. **81**, 865 (2009), arXiv: quant-ph/0702225

[2] A. Einstein, B. Podolsky, and N. Rosen, Phys. Rev. **47**, 777 (1935)

[3] J. S. Bell, Physics Physique Fizika **1**, 195 (1964)

[4] Y. Afik and J. R. M. n. de Nova, Quantum **6**, 820 (2022), arXiv: 2203.05582[quant-ph]

[5] R. Aoude, H. Banks, C. D. White *et al.*, (2025), arXiv: 2505.12522 [hep-ph]

[6] Y. Afik *et al.*, (2025), arXiv: 2504.00086 [hep-ph]

[7] Y. Fang, C. Gao, Y.-Y. Li *et al.*, Sci. China Phys. Mech. Astron. **68**, 260301 (2025), arXiv: 2411.11294[hep-ph]

[8] E. Gabrielli and L. Marzola, Symmetry **16**, 1036 (2024), arXiv: 2408.05010[hep-ph]

[9] M. Fabbrichesi, R. Floreanini, E. Gabrielli *et al.*, Phys. Rev. D **110**, 053008 (2024), arXiv: 2406.17772[hep-ph]

[10] M. Fabbrichesi, R. Floreanini, E. Gabrielli *et al.*, Phys. Rev. D **109**, L031104 (2024), arXiv: 2305.04982[hep-ph]

[11] R. von Kuk, K. Lee, J. K. L. Michel *et al.*, (2025), arXiv: 2503.22607 [hep-ph]

[12] Y. Afik and J. R. M. n. de Nova, Eur. Phys. J. Plus **136**, 907 (2021), arXiv: 2003.02280[quant-ph]

[13] Y. Afik, Y. Kats, J. R. M. n. de Nova *et al.*, (2024), arXiv: 2406.04402 [hep-ph]

[14] M. Fabbrichesi, R. Floreanini, and G. Panizzo, Phys. Rev. Lett. **127**, 161801 (2021), arXiv: 2102.11883[hep-ph]

[15] Y. Afik and J. R. M. n. de Nova, Phys. Rev. Lett. **130**, 221801 (2023), arXiv: 2209.03969[quant-ph]

[16] C. Severi, C. D. E. Boschi, F. Maltoni *et al.*, Eur. Phys. J. C **82**, 285 (2022), arXiv: 2110.10112[hep-ph]

[17] J. A. Aguilar-Saavedra and J. A. Casas, Eur. Phys. J. C **82**, 666 (2022), arXiv: 2205.00542[hep-ph]

[18] R. Aoude, E. Madge, F. Maltoni *et al.*, Phys. Rev. D **106**, 055007 (2022), arXiv: 2203.05619[hep-ph]
[19] T. Han, M. Low, and T. A. Wu, JHEP **07**, 192 (2024), arXiv: 2310.17696[hep-ph]
[20] Z. Dong, D. Gon?calves, K. Kong *et al.*, Phys. Rev. D **109**, 115023 (2024), arXiv: 2305.07075[hep-ph]
[21] C. Severi and E. Vryonidou, JHEP **01**, 148 (2023), arXiv: 2210.09330[hep-ph]
[22] F. Maltoni, C. Severi, S. Tentori *et al.*, JHEP **09**, 001 (2024), arXiv: 2404.08049[hep-ph]
[23] J. A. Aguilar-Saavedra, Phys. Rev. D **109**, 096027 (2024), arXiv: 2401.10988[hep-ph]
[24] J. A. Aguilar-Saavedra, Phys. Lett. B **855**, 138849 (2024), arXiv: 2402.14725[hep-ph]
[25] K. Cheng, T. Han, and M. Low, Phys. Rev. D **111**, 033004 (2025), arXiv: 2407.01672[hep-ph]
[26] G. Aad *et al.* (ATLAS), Nature **633**, 542 (2024), arXiv: 2311.07288 [hep-ex]
[27] A. Hayrapetyan *et al.* (CMS), Rept. Prog. Phys. **87**, 117801 (2024), arXiv: 2406.03976 [hep-ex]
[28] A. Hayrapetyan *et al.* (CMS), Phys. Rev. D **110**, 112016 (2024), arXiv: 2409.11067 [hep-ex]
[29] A. G. White, D. F. V. James, P. H. Eberhard *et al.*, Phys. Rev. Lett. **83**, 3103 (1999)
[30] D. F. V. James, P. G. Kwiat, W. J. Munro *et al.*, Phys. Rev. A **64**, 052312 (2001)
[31] R. T. Thew, K. Nemoto, A. G. White *et al.*, Phys. Rev. A **66**, 012303 (2002)
[32] S. Popescu and D. Rohrlich, Found. Phys. **24**, 379 (1994)
[33] A. J. Barr, M. Fabbrichesi, R. Floreanini*et al.*, Prog. Part. Nucl. Phys. **139**, 104134 (2024), arXiv: 2402.07972[hep-ph]
[34] J. C. Martens, J. P. Ralston, and J. D. Tapia Takaki, Eur. Phys. J. C **78**, 5 (2018), arXiv: 1707.01638[hep-ph]
[35] A. Bernal, Phys. Rev. D **109**, 116007 (2024), arXiv: 2310.10838[hep-ph]
[36] J. A. Aguilar-Saavedra and J. Bernabeu, Phys. Rev. D **93**, 011301 (2016), arXiv: 1508.04592[hep-ph]
[37] J. A. Aguilar-Saavedra, Phys. Rev. D **107**, 076016 (2023), arXiv: 2209.14033[hep-ph]
[38] J. A. Aguilar-Saavedra, A. Bernal, J. A. Casas*et al.*, Phys. Rev. D **107**, 016012 (2023), arXiv: 2209.13441[hep-ph]
[39] R. Ashby-Pickering, A. J. Barr, and A. Wierzchucka, JHEP **05**, 020 (2023), arXiv: 2209.13990[quant-ph]
[40] A. J. Barr, Phys. Lett. B **825**, 136866 (2022), arXiv: 2106.01377[hep-ph]
[41] A. J. Larkoski, Phys. Rev. D **105**, 096012 (2022), arXiv: 2201.03159[hep-ph]
[42] M. Fabbrichesi and L. Marzola, Phys. Rev. D **110**, 076004 (2024), arXiv: 2405.09201[hep-ph]
[43] K. Ma and T. Li, Chin. Phys. C **48**, 103105 (2024), arXiv: 2309.08103[hep-ph]
[44] S. Fedida and A. Serafini, Phys. Rev. D **107**, 116007 (2023), arXiv: 2209.01405[quant-ph]
[45] M. Fabbrichesi, R. Floreanini, E. Gabrielli *et al.*, JHEP **09**, 195 (2023), arXiv: 2304.02403[hep-ph]
[46] T. Han, M. Low, and Y. Su, (2025), arXiv: 2501.04801 [hep-ph]
[47] K. Cheng and B. Yan, (2025), arXiv: 2501.03321 [hep-ph]
[48] M. Grossi, G. Pelliccioli, and A. Vicini, JHEP **12**, 120 (2024), arXiv: 2409.16731[hep-ph]
[49] K. Cheng, T. Han, and M. Low, (2024), arXiv: 2410.08303 [hep-ph]
[50] T. Han, M. Low, N. McGinnis *et al.*, (2024), arXiv: 2412.21158 [hep-ph]
[51] D. Gon¸calves, A. Kaladharan, F. Krauss *et al.*, (2025), arXiv: 2505.12125 [hep-ph]
[52] M. Del Gratta, F. Fabbri, P. Lamba *et al.*, (2025), arXiv: 2504.03841 [hep-ph]
[53] S. L. Glashow, Nucl. Phys. **22**, 579 (1961)
[54] P. W. Higgs, Phys. Rev. Lett. **13**, 508 (1964)
[55] A. Salam and J. C. Ward, Phys. Lett. **13**, 168 (1964)
[56] S. Weinberg, Phys. Rev. Lett. **19**, 1264 (1967)
[57] H. Al Ali *et al.*, Rept. Prog. Phys. **85**, 084201 (2022), arXiv: 2103.14043[hep-ph]
[58] M. Boscolo, J.-P. Delahaye, and M. Palmer, Rev. Accel. Sci. Tech. **10**, 189 (2019), arXiv: 1808.01858[physics.acc-ph]
[59] F. Mintert, M. Ku′s, and A. Buchleitner, Phys. Rev. Lett. **92**, 167902 (2004)
[60] H. Ollivier and W. H. Zurek, Phys. Rev. Lett. **88**, 017901 (2001), arXiv: quant-ph/0105072
[61] S. Bravyi and A. Kitaev, Phys. Rev. A **71**, 022316 (2005), arXiv: quant-ph/0403025
[62] M. Srednicki, Phys. Rev. Lett. **71**, 666 (1993), arXiv: hep-th/9303048
[63] M. Gell-Mann, Phys. Rev. **125**, 1067 (1962)
[64] C. H. Bennett, D. P. DiVincenzo, J. A. Smolin *et al.*, Phys. Rev. A **54**, 3824 (1996), arXiv: quantph/9604024
[65] W. K. Wootters, Phys. Rev. Lett. **80**, 2245 (1998), arXiv: quant-ph/9709029
[66] F. Mintert and A. Buchleitner, Physical review letters **98**, 140505 (2007)
[67] K. Chen, S. Albeverio, and S.-M. Fei, Phys. Rev. Lett. **95**, 040504 (2005)
[68] R. Rahaman and R. K. Singh, Nucl. Phys. B **984**, 115984 (2022), arXiv: 2109.09345[hep-ph]
[69] J. A. Aguilar-Saavedra, J. Bernab′eu, V. A. Mitsou *et al.*, Eur. Phys. J. C **77**, 234 (2017), arXiv: 1701.03115[hep-ph]
[70] S. Navas *et al.* (Particle Data Group), Phys. Rev. D **110**, 030001 (2024)
[71] J. Alwall, R. Frederix, S. Frixione *et al.*, JHEP **2014**, 1 (2014)
[72] P. Artoisenet, R. Frederix, O. Mattelaer, and R. Rietkerk, JHEP **03**, 015 (2013), arXiv: 1212.3460[hep-ph]
[73] S. Frixione, E. Laenen, P. Motylinski, and B. R. Webber, JHEP **04**, 081 (2007), arXiv: hep-ph/0702198
[74] R. D. Ball *et al.*, Nucl. Phys. B **867**, 244 (2013), arXiv: 1207.1303[hep-ph]
[75] M. Fabbrichesi, R. Floreanini, E. Gabrielli *et al.*, Eur. Phys. J. C **83**, 823 (2023)
[76] R. Ashby-Pickering, A. J. Barr, and A. Wierzchucka, JHEP **2023**, 1 (2023)